Experimental Mechanics (2022) 62:885–888
https://doi.org/10.1007/s11340-022-00833-x

BRIEF TECHNICAL NOTE

# Algorithms for Nanoindentation Strain Rate Jump Testing and Analysis

**K. M. Schmalbach**[1] · **N. A. Mara**[1,1]

Received: 9 September 2021 / Accepted: 24 February 2022 / Published online: 10 March 2022


## Abstract

**Background** Understanding the dynamics of deformation processes is of interest for determining the dominant thermally activated processes during plasticity [1] and fracture [2, 3]. Strain rate jump (SRJ) tests have been recently introduced to investigate intrinsic deformation mechanisms and have been successfully utilized on some nanomechanical test platforms [4–6].
**Objective** The goal is to create standardized SRJ testing and analysis protocols for Hysitron nanoindenters, which cannot be found in literature, besides our previous work [7].
**Methods** Presented here is software to create SRJ test load functions for the TI980, which could be adapted to other instruments, and standardized protocols for analyzing the associated data.
**Results** These protocols are validated using single crystal tungsten as a model material and agree well with literature values from other instruments.
**Conclusions** New freely available software, validated on single crystal tungsten, creates opportunities for others to investigate intrinsic deformation mechanisms in more complex systems.

**Keywords** Hysitron TI980 · Triboindenter 980 · Mechanical properties · Mechanical testing · Strain rate sensitivity · Activation volume

## Theory

For pyramidal indenters, the indentation strain rate, $\dot{\varepsilon}$, is strictly defined as the ratio of the indenter displacement rate to current displacement, $\frac{\dot{h}}{h}$, and is analogous to the engineering strain rate in a tensile or compression experiment [4]. For load-controlled indentation, however, it is more useful to represent this as $\dot{\varepsilon} = \frac{\dot{h}}{h} = \frac{1}{2}\left(\frac{\dot{P}}{P} - \frac{\dot{H}}{H}\right)$, where $\dot{P}$ is the time derivative of the load and $\dot{H}$ is the time derivative of the hardness. If the hardness is not changing, this simplifies to:

$$\dot{\varepsilon} \approx \frac{1}{2}\frac{\dot{P}}{P} \tag{1}$$

In the TI980, the load function is a list of desired loads and the times at which those loads should be applied. An analytical expression for the load as a function of time is therefore required. Rearranging and integrating equation (1) gives

$$P = P_0 \exp\{2\dot{\varepsilon}\left(t - t_0\right)\} \tag{2}$$

to define the load as a function of time for a given strain rate segment. Here, $P_0$ and $t_0$ are the load and time at the start of the constant strain rate segment. This can be applied consecutively to yield a load function with several constant strain rate segments in series, i.e. a strain rate jump test. One can minimize the duration of a test by beginning with a faster strain rate such that the lower strain rate segments begin at a high $P_0$. Additionally, performing a strain rate jump test results in far greater data density than multiple constant strain rate experiments, while reducing the effect of site-to-site variability.

Following the test, the strain rate sensitivity can be calculated by [8]:

$$m = \frac{\partial \ln H}{\partial \ln \dot{\varepsilon}} \tag{3}$$

✉ N. A. Mara
mara@umn.edu

K. M. Schmalbach
schma174@umn.edu

[1] Department of Chemical Engineering and Materials Science, University of Minnesota, Minneapolis, MN 55455, USA

where m is the strain rate sensitivity (SRS), H is the hardness, $\dot{\epsilon}$ is the strain rate, and ln is the natural logarithm. The activation volume was calculated by [5]:

$$V^* = C^* \sqrt{3} kT \frac{\partial \ln(\dot{\epsilon})}{\partial H} \tag{4}$$

where V* is the activation volume, C* is the constraint (Tabor) factor, commonly assumed to be 3 [9], k is the Boltzmann constant, T is the absolute temperature (here, 300 K), $\dot{\epsilon}$ is the strain rate, and H is the hardness.

Some of the effects associated with high strain rate, e.g. plasticity error, can be corrected for with post-processing of the data [6]. The approach uses a known tip area function and a known reduced modulus ($E_r$, from separate nanoindentation experiments) to calculate the corrected contact depth via numerical solution of a set of nonlinear equations:

$$S = 2\beta E_r \sqrt{\frac{A_c}{\pi}} \tag{5}$$

$$h_c = h - \epsilon \frac{P}{S} \tag{6}$$

$$A_c = c_0 h_c^2 + c_1 h_c + c_2 h_c^{\frac{1}{2}} + c_3 h_c^{\frac{1}{4}} + c_4 h_c^{\frac{1}{8}} + c_5 h_c^{\frac{1}{16}} \tag{7}$$

where the only unknowns are stiffness (S), contact area ($A_c$), and contact depth ($h_c$). The indentation size effect (ISE) can be modeled using the theory developed by Nix and Gao [10] by rearrangement for $H_0$, the hardness at infinite depth:

$$H_0 = \frac{H}{\sqrt{1 + \frac{h^*}{h_c}}} \tag{8}$$

where H is the hardness, $h_c$ is the contact depth, both corrected for plasticity error, and h* is the characteristic length scale, approximately 300 nm, as determined from regression with the Nix-Gao model on constant strain rate data performed at low strain rate ($10^{-2}$ $s^{-1}$).

## Experimental Procedure

A rod of single crystal tungsten was sectioned into semicircular prismatic pieces with two orthogonal (100)-type faces. The top surface was polished to 1200 grit smoothness with SiC paper on a polishing wheel prior to electropolishing in an ice-cold 2 wt% sodium hydroxide solution. The counter electrode was stainless steel, and the electropolishing voltage was held at 8.0 V. The resulting RMS surface roughness was 15.0 nm as determined by scanning probe microscopy using a TI980 nanoindenter with a Berkovich probe.

A strain rate jump test load function, as plotted in Fig. 1(a), was created with our freely available Python-based load function generator using seven consecutive strain rate segments with the following strain rates: $5\times10^{-1}$, $10^{-1}$, $10^{-2}$, $10^{-3}$, $10^{-2}$, $10^{-1}$, and $5\times10^{-1}$ $s^{-1}$. All segments use the continuous stiffness measurement (CSM) approach with an oscillation frequency of 70 Hz and a displacement amplitude of approximately 0.9 nm. The tungsten crystal was mounted with cyanoacrylate glue to a magnetic AFM disc and glued to the stage of a Hysitron Triboindenter 980 (Bruker Nanosurfaces, Minneapolis, MN) equipped with a 3D Omniprobe indenter head, having a maximum load of 10 N. The tip shape (contact area function) was calibrated via the Oliver and Pharr method using a fused silica standard with a diamond Berkovich tip [11].

A series of MATLAB functions, the theory of which is presented above, was created for post-processing of the data. These include (1) zeroing of the load and displacement; (2) cutting the data from the hold and the unload, where CSM is not used; (3) cutting the data from the low displacement region, where tip area function uncertainties dominate; (4) calculation of the contact depth and contact area based on a reference reduced modulus, as presented by Merle et al. [6]; and (5) correction for the ISE using the model of Nix and Gao [10]. A final function is used to evaluate the strain rate sensitivity discretely by identifying the plateau in hardness, extrapolating to the depth at which the jump occurred (in the event of a plateau that has a slight non-zero slope), and calculating the change in hardness discretely, as displayed in Fig. 2(c).

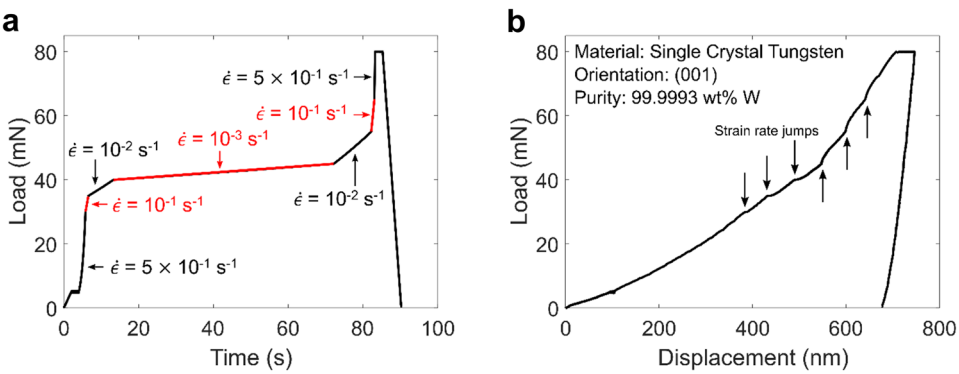


**Fig. 1** (**a**) Load function generated with the above-described editor with strain rates marked. (**b**) Load–displacement response from a strain rate jump test on single crystal tungsten. Arrows indicate the change in behavior associated with a change in strain rate

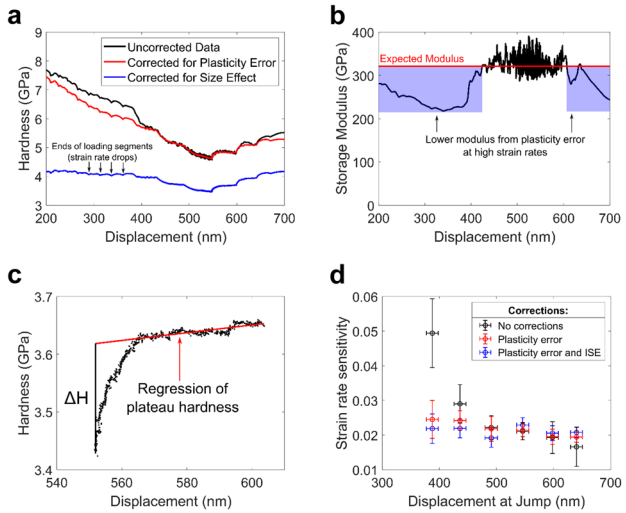


**Fig. 2** (**a**) Hardness profile from a strain rate jump test before corrections (black), after corrections for plasticity error (red), and after correcting for both plasticity error and ISE (blue); (**b**) storage modulus profile showing the large error associated with high strain rate, requiring correction; (**c**) Higher magnification of a single strain rate segment from a SRJT. The ΔH indicates the change in hardness used in equations (3) and (4) to calculate m and V*, respectively; (**d**) Effect of corrections on calculated strain rate sensitivity. Plasticity error contributes significant error to the calculation, whereas size effect contributes differences that decrease with increasing depth

## Results and Discussion

One can determine the effect of a change in strain rate by observing the load–displacement response; a change in slope in the load–displacement response should be present when the indentation strain rate is changed. As can be seen in Fig. 1(b), there is a clear change in the slope when the strain rate is changed. There is first a short transient region with rapidly changing slope, followed by a new steady state regime. For materials with a positive strain rate sensitivity, the loading curves exhibit a decreasing slope when decreasing strain rate, as would be expected from a softer response. The inverse is true when increasing the strain rate.

A quantitative look at the depth dependence of the hardness can be seen in the black curve in Fig. 2(a), where the hardness calculated via the Oliver and Pharr method [11] has only been further altered by correcting the zero (contact) point of the load–displacement curve. The first thing to notice is the very high apparent hardness in the first strain rate segment; the strain rate during this segment is $5\times10^{-1}$ $s^{-1}$, a strain rate at which plasticity error is expected. A look at the storage modulus (Fig. 2(b)), a reduced modulus, confirms the presence of considerable error during the first and last strain rate segments (200–375 and 625–700 nm) with the highest strain rate. Performing a correction by solving for the true contact depth using the area function and known reduced modulus of tungsten (320 GPa for a diamond indenter) results in the hardness profile seen in the red curve in Fig. 2(a). Here, the change in hardness between the first and second strain rates is much more similar to that seen at other strain rate jumps than before this correction was applied. The correction has little effect at low strain rates, as expected, due to the lack of plasticity error. These differences are due to the ISE discussed previously [5, 10], which is removed in the blue curve in Fig. 2(a). Removal of the ISE results in a flat hardness profile at constant strain rate. Of note is that to achieve a plateau value of hardness, each strain rate only requires relatively short depth intervals such that only shallow indentations need be performed. A test using similar dynamic parameters, but at lower strain rates (to mitigate plasticity error) and to greater depths (to get past the indentation size effect) can be seen in the Supplementary Information (Figs. S1-S2), providing similar results between shallow indents using corrections and deep indents without corrections.

An additional feature to note is the repeated drop in the hardness at high strain rate, as indicated by the arrows in Fig. 2(a). This effect is due to the approximation of the exponential curve seen in equation (2) with linear segments; each drop results from an effective drop in strain rate as the linear segment diverges from the "ideal" exponential loading, resulting in a lower hardness and a discontinuity in the plot. The drops could be minimized by decreasing the time of each loading segment, currently performed by increasing the oscillation frequency. Currently, the maximum frequency of the 3D Omniprobe is 100 Hz; these data are already approaching the upper bound, and 100 Hz was not sufficient to eliminate the drops. Shorter load segments, and thus better strain rate control, may be feasible using the high acquisition rate of raw load and displacement data combined with a known reduced modulus and area function, as is already used in the correction for plasticity error employed here.

The developed analysis functions were used to calculate the change in hardness at each strain rate jump as indicated in Fig. 2(c). The change in hardness is used in equations (3) and (4) to calculate the SRS and V*. Additionally, Fig. 2(d) displays the measured SRS as a function of depth when calculated with each of the sets of data corrections previously discussed. As can be seen, corrections for plasticity error are crucial to accurately depicting the SRS of a material, while ISE corrections are more minor. However, the combination of data corrections allows a wider range of strain rates to be used and to much lower depths, such that these techniques can be applied to a wide range of materials. As Fig. 2(d) shows, the SRS is nearly constant as a function of depth due to the corrections. Averaging over all 25 tests and 6 strain rate jumps results in a mean SRS of 0.021 with a standard deviation of 0.0023, nearly identical to that reported in the literature as tested by other means [12]. These results thereby validate the use of these tools for making load functions and analyzing the resulting data.

## Conclusions

Presented here is openly available software for creation of constant strain rate or strain rate jump test load functions designed for use with the Bruker Hysitron TI980 nanoindenter and adaptable to other instruments. The load–displacement response shows clear changes with changing strain rate. The measured hardness also changes significantly with strain rate, as expected. However, the hardness is vastly overestimated at high strain rates, which can be corrected for post-indentation. Finally, the strain rate sensitivity and activation volume are close to what have been reported in literature, validating the presented protocols.

**Supplementary Information** The online version contains supplementary material available at https://doi.org/10.1007/s11340-022-00833-x.

**Funding** Parts of this work were carried out in the Characterization Facility, University of Minnesota, which receives partial support from NSF through the MRSEC program. NAM and KMS acknowledge support by DOE-NE's Advanced Fuels Campaign through a Los Alamos National Laboratory subcontract number 536246.

## Declarations

**Conflict of Interest Statement** The authors declare that there is no conflict of interest.

**Notes** The software is maintained at https://github.com/KSchmalbach/IndentationAnalysis

## References

1. Weinberger CR, Boyce BL, Battaile CC (2013) Slip planes in bcc transition metals. Int Mater Rev 58:296–314. https://doi.org/10.1179/1743280412Y.0000000015
2. Hintsala ED, Teresi C, Wagner AJ et al (2014) Fracture transitions in iron: Strain rate and environmental effects. J Mater Res 29:1513–1521. https://doi.org/10.1557/jmr.2014.142
3. Gerberich WW, Schmalbach KM, Chen Y et al (2021) Quantifying physical parameters to predict brittle/ ductile behavior. Mater Sci Eng A 808:140899. https://doi.org/10.1016/j.msea.2021.140899
4. Lucas BN, Oliver WC (1999) Indentation power-law creep of high-purity indium. Metall Mater Trans A 30:601–610. https://doi.org/10.1007/s11661-999-0051-7
5. Maier V, Schunk C, Göken M, Durst K (2015) Microstructure-dependent deformation behaviour of bcc-metals – indentation size effect and strain rate sensitivity. Philos Mag 95:1766–1779. https://doi.org/10.1080/14786435.2014.982741
6. Merle B, Higgins WH, Pharr GM (2020) Extending the range of constant strain rate nanoindentation testing. J Mater Res 35:343–352. https://doi.org/10.1557/jmr.2019.408
7. Schmalbach KM, Lin AC, Bufford DC et al (2021) Nanomechanical mapping and strain rate sensitivity of microcrystalline cellulose. J Mater Res 36:2251–2265. https://doi.org/10.1557/s43578-021-00138-0
8. Maier V, Durst K, Mueller J et al (2011) Nanoindentation strain-rate jump tests for determining the local strain-rate sensitivity in nanocrystalline Ni and ultrafine-grained Al. J Mater Res 26:1421–1430. https://doi.org/10.1557/jmr.2011.156
9. Tabor D (1951) The Hardness of Metals
10. Nix WD, Gao H (1998) Indentation size effects in crystalline materials: A law for strain gradient plasticity. J Mech Phys Solids 46:411–425. https://doi.org/10.1016/S0022-5096(97)00086-0
11. Oliver WC, Pharr GM (1992) An improved technique for determining hardness and elastic modulus using load and displacement sensing indentation experiments. J Mater Res 7:1564–1583. https://doi.org/10.1557/JMR.1992.1564
12. Kappacher J, Leitner A, Kiener D et al (2020) Thermally activated deformation mechanisms and solid solution softening in W-Re alloys investigated via high temperature nanoindentation. Mater Des 189:108499. https://doi.org/10.1016/j.matdes.2020.108499